

Bubble clustering and trapping in large vortices. Part 1: Triggered bubbly jets investigated by phase-averaging

Rade Ž. Milenković^{a,*}, Beat Sigg^b, George Yadigaroglu^{b,1}

^a *Laboratorium für Thermohydraulik, Paul Scherrer Institut, CH-5232 Villigen PSI, Switzerland*

^b *Former Laboratorium für Kerntechnik, ETHZ, CH-8092 Zürich, Switzerland*

Received 31 August 2006; received in revised form 17 March 2007

Abstract

The characteristics of large coherent structures in turbulent, periodically-excited, as well as naturally-developing bubbly jets are investigated, and interactions between bubbles and large-scale vortices are studied quantitatively.

As information on size and development of the large-eddy structures is very difficult to obtain in naturally-developing flows, periodical excitation of the jet with frequencies in the neighbourhood of natural instabilities is applied to systematically create large coherent structures. When bubbles enter such vortices, they can be trapped if certain conditions are fulfilled; a trapping criterion is developed.

To study trapping phenomena, simultaneous two-phase PIV (particle image velocimetry), DOS (double optical sensors), LIF (laser induced fluorescence) and photographic techniques were applied for tracking the large vortices and bubble structures. In order to quantify the interaction between bubbles and the large vortices that are formed in the shear layer, characteristic phase-averaged quantities were determined by PIV and DOS.

© 2007 Elsevier Ltd. All rights reserved.

Keywords: Bubbly jets; Excited jets; Coherent structures; Bubble trapping; PIV; Optical probes; Phase averaging; Ensemble averaging

1. Introduction

A number of experimental, theoretical and computational investigations of usually quasi-fully-developed multiphase flows have already been conducted to improve the understanding of complex multiphase flow phenomena. Even simplified topological sketches of the different two-phase flow patterns immediately give rise to many questions that cannot be easily answered. The mathematical treatment of such multidimensional gas–liquid flows is very complicated and requires adequate models for the exchange of mass, momentum and heat

* Corresponding author. Present address: University of Applied Sciences – Northwestern Switzerland, Institute for Thermal and Fluid Engineering, Klosterzelgstrasse 2, CH-5210 Windisch, Switzerland. Tel.: +41 56 462 45 40; fax: +41 56 462 44 15.

E-mail addresses: rvmil@bluewin.ch, rade.milenkovic@fhnw.ch (R.Ž. Milenković).

¹ Present address: ETH WEN B-13, Weinbergstrasse 94, CH-8006 Zürich, Switzerland.

between the phases. In particular, the modelling of turbulence (shear-induced and bubble-induced turbulence), of turbulence characteristics such as fluctuating velocities, of autocorrelation functions and integral scales of turbulence, of forces acting on gas flow structures, of phase interactions, of the time-dependent shape and size of gas–liquid flow structures, of any effects of surfactants and of the interaction between gas and liquid flow structures are subjects of special interest.

Since one of the objectives of this paper is to analyze coherent structures of liquid and bubbles in bubbly jets, especially by making use of triggering techniques for producing periodically developing vortex structures in the jet, a short survey of pertinent work on the subject is given. Most research has, of course, been conducted with single-phase jets; we review these publications first.

There are two types of jet instabilities, the shear-layer mode and the jet-column mode (Zaman and Hussain, 1980; Hussain, 1983). These two distinct modes characterize the conditions for vortex development in the near field of circular jets.

The first mode is attributed to the instability of the shear layer forming at the jet exit. This mode may be convective or absolute (Huerre and Monkewitz, 1985), where absolute instabilities can be important for jets with void fractions above 30%. For the present experiments, only the convective mode is of interest.

The second mode, called jet-column mode, is characterized by a Strouhal number scaled by the jet diameter D . The preferred mode leads to the formation of large vortices with Strouhal numbers $St = \frac{fD}{V_{\text{jet}}} \approx 0.3$ (f is the excitation frequency and V_{jet} is the mean superficial liquid velocity of the jet at the nozzle exit) in the downstream region of y/D between 2 and 6; y is the axial coordinate (Hussain and Zaman, 1981; Crow and Champagne, 1971). This mode is called preferred because the first maximum of the centreline vertical-velocity fluctuation, which occurs at four jet diameters from the jet exit, corresponds to this mode. Periodical triggering of this or any other mode allows one to produce large coherent structures in the jet. By phase-locking the measuring equipment to the triggering mechanism, it is possible to analyze coherent structures at various phases of development (Hussain and Zaman, 1980; Zaman and Hussain, 1980).

Experiments with buoyant, turbulent, single-phase jets were performed by Papanicolaou and List (1988), and the effect of periodic forcing on mixing in neutral and buoyant jets was analyzed by Mastorakos et al. (1996). It was found that higher levels of forcing (triggering intensity) were required for turbulent jets than for laminar ones and that a maximum enhancement of jet mixing with ambient fluid resulted for $St = 0.6$, which might have been the consequence of pairing induced by triggering a harmonic together with the basic mode.

The importance of the large-scale coherent structures producing interactions between the dispersed and the continuous phase was recognized long ago and was mainly investigated experimentally in planar free shear layers. Previous analytical work (Ruetsch and Meiburg, 1993) on bubble motion in both isolated vortices and in temporally-evolving shear layers showed that there is a stable equilibrium point at the vortex center when the bubble rise velocity is equal to zero. In analytical work (Sene et al., 1994) the effects of the trapping parameter of the jet shear layer and of the Jet Froude number on the bubble-trapping condition were examined.

More recently published experimental (Rightley and Lasheras, 2000) and numerical work (Druzhinin and Elghobashi, 2001) on bubble dispersion in planar free shear layers have shown that the presence of large-scale structures dominates the dispersion of the bubbles and the energy redistribution within the continuous phase. An experimental study (Rightley and Lasheras, 2000) of the dispersion of micro bubbles (50 μm) inside a planar shear layer with very weak forcing (and therefore, corresponding to the naturally-developing shear layer) provided information on the distribution of the experimentally determined inter-phase momentum transfer integral which includes the cumulative influence of all terms in the equation of bubble motion on to the continuous phase. It was shown that the presence of bubbles enhances the kinetic energy of the continuous phase and that its redistribution across the mixing layer occurs inhomogeneously. The experiment has not provided significant entrapping of the bubbles inside large coherent structures. The Strouhal number of the most amplified frequency was 0.032, which is below the forcing frequencies used during the experimental investigations presented here.

DNS simulation of a 3D bubbly mixing layer (Druzhinin and Elghobashi, 2001) showed an increment of bubble concentration close to the vortex centres as well as inside the rollers generated by vortex pairing in the core of the mixing layer. In addition, analysis of the instantaneous two-way coupling source term in

the equation of the spanwise vorticity showed that bubbles modified the vorticity field by creating neighbouring regions of enhanced or reduced vorticity.

To contribute to the understanding of complex two-phase phenomena and to provide experimental information, especially regarding coherent structures, a completely new experimental installation was built and used to collect extensive experimental data sets. The main goal of our investigations was to reveal the characteristics of large coherent structures in turbulent, periodically-excited as well as in naturally-developed, *bubbly jet flows*.

In the triggered-jet experiments, the shear layer at the jet exit is excited by a small external surging flow with controllable frequency and amplitude. At the same time, bubbles of uniform size are injected in a controllable jet flow and tracked with a novel method developed for this purpose. Simultaneous two-phase PIV and photographic techniques open another promising chapter in exploring two-phase flow phenomena. Thus the interaction between coherent structures and bubbles, as well as the feedback of bubble agglomeration on the development of these structures can be studied.

2. The experiment

The basic idea of this experiment (Milenkovic, 2005) is to create large, orderly structures in a bubbly jet with controllable frequency and phase, in order to enable their study by statistical means, in particular by performing phase or conditional ensemble averages, and to provide well-controlled conditions for investigating the interactions between the dispersed (bubbles) and the continuous phase (liquid). Periodical excitation of the jet at frequencies in the neighbourhood of natural instabilities is applied to systematically create large coherent structures and to demonstrate their importance. When bubbles enter such vortices, they can be trapped if certain conditions are fulfilled. The advantage of this approach is that the large, orderly vortices that appear with controllable frequency in the shear layer and the uniformly-sized bubbles that can be generated with controlled diameter create bubble movements that can be systematically observed. Such movements are difficult to analyze in naturally-developing two-phase jet flows.

A photo that illustrates a vortex ring in a single-phase jet is presented in Fig. 1. It was obtained by a LIF (Laser-Induced Fluorescence) technique (Milenkovic, 2005). The pixel gray level in the photograph corresponds to dye concentration. Based on this photo the following conclusions can be drawn:

- The measured distance between two consecutive vortex rings corresponds to the excitation period. Therefore, it is possible to roughly estimate the vortex vertical velocity and the size of the vortices at different positions.

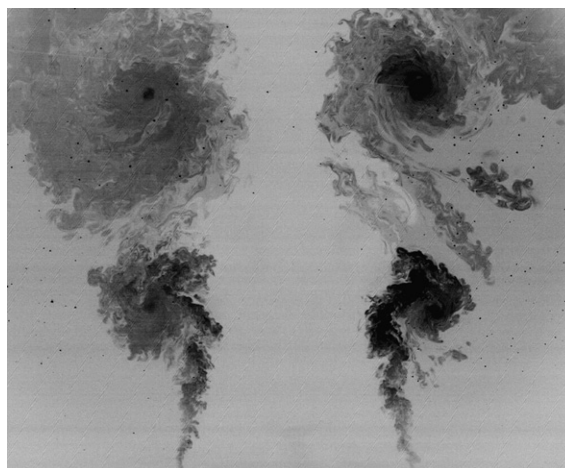


Fig. 1. Photos of the vortex rings obtained by LIF. Pixel values are inverted in order to achieve better contrast. Two vortex rings can be observed. The small black dots are the seeding particles used for the PIV measurements.

- There is a peak of the pixel grey-level value close to the centre of the vortices, which can be clearly observed for a second vortex ring. The distribution of the grey-level values across these vortices has an approximately Gaussian shape (Milenkovic, 2005).

The positions of the section of the large vortices further downstream are no longer symmetric, because of vortex ring deformations caused by instabilities in the shear layer.

In the case of bubbly flows, an interesting question arising is whether bubbles can be “trapped” in large vortices of the liquid flow field and if bubble clusters would be formed by the vortex structures. Thus, an attempt was made to show whether bubble clustering or trapping can be demonstrated in case of naturally-developing jets by DOS and PIV. If these techniques are applied in a standard way, only the spatial distribution of local statistical quantities can be measured. Since bubble clustering and trapping in case of naturally-developing jets are stochastic processes, it is very difficult to deduce relevant information regarding size of the structures, azimuthal vorticity distribution and bubble/liquid velocities across these structures from distributions of statistical properties. Therefore, it was decided to externally and periodically excite the bubbly jet.

The experiments have been carried out with a vertical water jet (called here single-phase jet) as well as a water jet containing bubbles of various well-controlled sizes and volume fractions (called here bubbly jet); the jet is injected into a water volume contained in a large Plexiglas tank to minimize wall effects. Unperturbed flows, with constant inlet flow rate of liquid and gas are here referred to as naturally-developing jets. If the jet flow is periodically excited with controlled frequency and amplitude, it is called triggered jet. The excitation is achieved by periodically modulating the jet shear layer by means of a coaxial water layer (EF) injected close to the jet exit through a separate nozzle (Fig. 2).

The gas/liquid injector and a schematic of the experiment (Milenkovic, 2005) are presented in Fig. 2. To produce the bubbly jet with uniform, but variable, bubble sizes, a special injector has been developed after a series of experiments carried out with different configurations (Milenkovic and Fehlmann, 2005). The optimal configuration of tubes and needles for forming bubbles with uniform size in the range between 1 and 6 mm was presented in more detail by Milenkovic and Fehlmann (2005). Bubbles are formed by continuously injecting air (AF) through the needles into the co-currently flowing internal liquid flow (ILF). The jet flow is formed afterwards by adding the second, external liquid flow (ELF).

The main dimensions of the experimental setup are:

- Diameter of the jet nozzle: $D = 90$ mm.
- Diameters of the injector tubes: $d_o/d_i = 4.0/3.4$ mm.
- Diameters of the excitation ring-nozzle: $D_o/D_i = 98/96$ mm.
- Number of injector tubes and needles: $N_{it} = 39$.
- Horizontal dimensions of the tank: $L = 1200 \times 1200$ mm.
- Height of the tank: $H = 2240$ mm.
- Water level in the tank: $H_L = 1200$ mm.

3. Experimental techniques

3.1. PIV (particle image velocimetry) and photographic techniques

In order to obtain time-averaged fields in case of naturally-developing jets, as well as phase-averaged velocity and vorticity fields at various phases of the triggering period (i.e., positions of the vortices in the flow field) in case of periodically triggered jets, a standard, commercial PIV system was used. It consists of a dual-cavity laser and two CCD cameras that work in a two-frame, double-exposure mode. A 2 mm laser light sheet illuminated a mid plane of the axisymmetric jet, while the two cameras with the beam splitter were aimed perpendicularly to the laser light sheet. The first camera with a green filter captured reflections from the bubbles, while the second camera with a red filter acquired the images with light emitted from the fluorescent seeding particles used in the experiment. These were 40 μm fluorescent (Rhodamine-B) particles. Therefore, the first

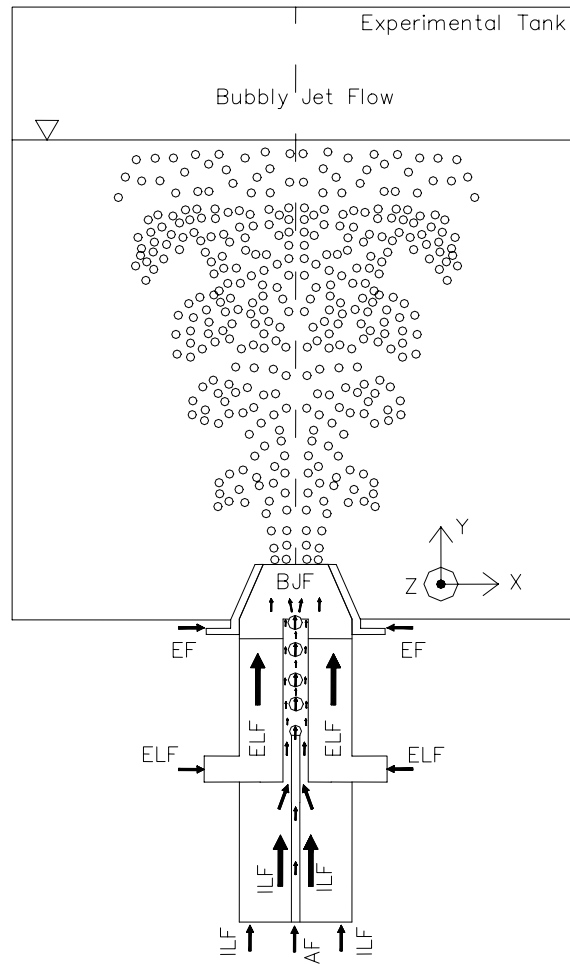


Fig. 2. Schematic of bubbly jet production. The injector shown at the bottom at a much larger scale has 39 injection needles (only one shown).

camera was used for the measurement of bubble velocities, whereas the second one enabled measurement of liquid velocities. The dimensions of the fields of view used were 138×138 mm and 220×220 mm in different series of tests. For the smaller field of view, the optical resolution of 1 pixel corresponded to about $140 \mu\text{m}$, and the size of the chosen interrogation area (IA) was 64×64 pixels or about 9×9 mm. The same setting was used for obtaining velocity fields of the liquid and of the bubbles. The second field of view was used for estimating the velocity of the vortex and of the bubble ring discussed later. The time between two laser pulses was adjusted to obtain a maximum particle displacement of less than 16 pixel (i.e., 25% of the IA). The error in velocity measurements corresponded to about 1% of the maximum value, if the resulting displacement uncertainty is 0.1 pixel (Dantec, 2000).

Neither CFD (Computational Fluid Dynamics) methods nor experimental techniques like PIV produce results with infinitesimal resolution in space or time; both imply some inherent filtering. For a thorough discussion of experimental results obtained by PIV and their comparison with CFD results, it is therefore necessary to properly define and distinguish different filtered quantities. Filtering means that a time- and space-dependent quantity is multiplied with a weight function and integrated over an interval in time or space. The PIV signals can be decomposed into average and fluctuating components. An inherent characteristic of PIV results is that they are both filtered in space as well as in time. Space filtering in PIV is applied over the interrogation volume (area \times laser light sheet thickness). In PIV the size of the interrogation volume is roughly constant, which means that a constant size of the interrogation mesh is chosen for processing the

images. The successive image correlation technique applied for acquiring the average velocity in the IA provides an inherent space and time filtering, with the characteristic lengths: size of IA and time delay between two successive laser flashes.

The time steps in CFD and PIV have the same order of magnitude, although the criteria for their selection are, of course, different. In the case of two-phase flow a new fundamental problem arises. The selection of the PIV interrogation area depends on the bubble diameters and turbulent length scales to be resolved. The PIV method applied here was used for resolving the large eddy structures. The IA was large enough to contain one or more bubbles, as the PIV mesh size should not be smaller than the characteristic length scale of the dispersed phase, i.e., the bubble diameter.

Another question is whether the measured bubble velocity is correct if the bubble size is comparable to the IA size. The size of the interrogation area should be large enough to contain the strongest reflections of the bubbles in order to achieve sufficient statistical accuracy for estimating the cross-correlation function. For the same total intensity of laser light reflected from the bubbles in an IA, the reflections can consist of many small spots from several small bubbles or, at the other extreme, by one large patch from a large unique bubble. The cross-correlation function produced by the small bubbles is more strongly peaked (provided that bubble reflections patterns are very similar in the two consecutive exposures) than in the case of one large bubble. The statistical error of the velocity calculations might, therefore, increase with bubble size. Nevertheless, the reflections emitted by a relatively large bubble that extends over a considerable part of the IA exhibit a characteristic intensity structure which still leads to meaningful results of the peak of the cross-correlation function and thus the velocity calculation.

On the other hand, the size of the large structures that are visualized experimentally by PIV must be considerably larger than the size of the IA as well as that of the bubbles in order that interaction effects between large vortices and bubbles can be investigated. In particular, if the bubble trapping phenomenon is investigated, the size of the large vortices should obviously be considerably larger than the size of the bubbles to be tracked inside them.

Considering now the liquid velocity measurements for a successful application of the cross-correlation algorithm, the number of particles per IA should be at least 5 (Dantec, 2000). If an adequate seeding density is ensured, i.e., 5–10 particles per IA, the void areas caused by the presence of bubbles do not contribute significantly to the measurement errors; the liquid velocities remain cross-correlated averages over the IA occupied by the liquid and correctly do not include missing data from the areas occupied by the bubbles. Such an adequate seeding density for PIV measurements was achieved with our dosing system (Milenkovic, 2005).

A statistical analysis of PIV results (Raffel et al., 1998) requires an ensemble consisting of a large number of vector maps. Depending on the flow conditions, the basic PIV settings and, especially, the quality of feeding the flow with seeding particles, the number of rejected velocity vectors per vector map may vary. For the experiments with naturally-developing jets, performed at the constant acquisition frequency of 15 Hz, 1024 vector maps were acquired. Assuming that 50% of the vectors were accepted for a given point (an IA) in the shear layer (i.e., $N_v = 512$), the theoretical statistical error of the mean velocity is less than 2% for a standard deviation of the velocity measurements of 30% and about equal to the resolution error of the PIV measurements. The theoretical statistical error of the variance is less than 10%. A similar error analysis was presented by Ullum et al. (1998).

In addition to the PIV cameras, a third digital camera was used to capture pictures of bubbles and bubble structures, especially for the triggered experiments.

3.2. Vortex tracking

In order to obtain velocity and vorticity fields at various phases within the triggering period, showing different positions of the vortices in the flow field, a data acquisition scheme has been devised that is synchronized with the excitation of the jet. PIV acquisition is started by the periodic external signal from an encoder, which covers two excitation periods. The PIV recordings were acquired with higher frequency (in our cases 12 Hz or 15 Hz, depending on the excitation frequency). For instance, at the excitation frequency of 2 Hz, six shots per excitation period can be captured with a PIV acquisition rate of 12 Hz, allowing phase-averaging at six different times within the excitation period to be performed. The data acquired this

way yield information on deformations, size modifications and velocity of the vortex ring. This acquisition method, called here vortex tracking method, is a very useful tool for tracking large vortices in a flow field (Milenkovic, 2005; Milenkovic et al., 2005).

3.3. Double optical sensor (DOS) measurements

A standard instrument, often used in bubbly flows, is the double optical sensor. Void fraction (ε), number of bubbles (N), bubble chord-length distribution and vertical bubble velocity (V_B) can be measured by DOS. The double optical sensor used in our tests for void fraction and bubble velocity measurements was horizontally oriented and had a vertical distance between tips of $\Delta y_{\text{tips}} = 0.75$ mm; the tips were vertically aligned. Earlier tests done with this configuration were presented by Kubasch (2001). It was shown that sensor orientation has very little influence on the void fraction measurements and no effect on bubble frequency measurement for the range of bubble sizes investigated here. Comparison of bubble velocity measurements by PIV and DOS for turbulent flow conditions with high-bubble concentration (Milenkovic, 2005), showed that the velocities measured by DOS are larger than those obtained with PIV. As reported by Le Corre and Ishii (2002), an overestimation of the bubble velocity by up to 30% is expected for regions of the flow field where the bubble velocity fluctuations cannot be neglected. In general, the DOS-measured bubble velocities may be influenced by many factors such as sensor response, sensor geometry, bubble shape and bubble velocity fluctuations (Le Corre and Ishii, 2002).

The mean void fraction at a local position in the flow field is defined as the ratio between the time when air is present at the upstream sensor tip and the total measuring time; the mean void fraction is estimated by averaging the void signal over a long-time period.

The vertical component of the bubble velocity, V_B , is defined as the ratio between the tip separation distance and the measured time of flight. The bubble velocity is obtained by averaging over a suitably long-time that must be properly chosen to obtain statistically secured results. The data acquisition time varied between 300 and 600 s, depending on bubble concentration, making the vertical bubble velocity measurements long-time, local averages.

In order to perform phase averaging of the experimental results for void fraction and bubble velocity in case of triggered jets, the data acquisition was triggered again by the external encoder signal. An integer number of excitation periods (usually 6000 periods containing data) were recorded. Each excitation period was subdivided into an integer number of equal intervals. For instance, the excitation period of 0.5 s was divided into 25 intervals of 0.02 s. Bubble number, void fraction and bubble velocity data were averaged over the total number of periods for each of these intervals (ensemble average). The selected time resolution should be adequate for distinguishing trapped from non-trapped bubbles in phase-averaged void fraction and bubble velocity distributions. If, for instance, the velocity of the vortex ring displacement is about 0.27 m/s, the time interval of 0.02 s corresponds to a vertical displacement of a trapped bubble of about 5.5 mm. The void fraction generated by trapped bubbles would then be averaged over $\Delta y = 5.5$ mm, which is comparable to the bubble size. In addition, for regions with low-bubble concentration, i.e., the jet shear layer, the total number of periods for phase-averaging must be sufficient for statistically meaningful results.

4. Bubble movement and trapping in large shear-layer structures

In order to study interactions between bubbles and large eddies formed in the shear layer and especially bubble trapping phenomena, it is necessary to consider the equation of motion of a single bubble and to determine the velocity field of the liquid. Despite the fact that flow conditions for bubble trapping are in reality more complex, the approach presented here can be used to check whether the conditions for bubbles to reach an equilibrium position in large vortices are fulfilled.

4.1. Simplified condition for bubble trapping

For the derivation of a trapping criterion, a simplified cylindrical vortex with axis normal to the buoyancy direction moving uniformly in the x - y plane is considered and the forces acting on a single bubble are formu-

lated. Trapping of the bubble is then defined as the existence of an equilibrium position of the bubble inside the vortex. A more general form of trapping is that of a bubble moving relative to the vortex axis, but remaining inside the vortex (Sene et al., 1994; Magnaudet and Eames, 2000). More information on these criteria can be found in Section 5.1. Furthermore, in vortices tilted with respect to the direction of gravity, a trapped bubble would move along the vortex axis.

The large, coherent, toroidal vortices surrounding the jet travel vertically with about half the mean jet velocity (V_{jet}) (Crow and Champagne, 1971). For simplicity, these toroidal objects are replaced by cylindrical vortices with axis normal to the x - y plane in Fig. 3. It is assumed that their vorticity ω_z has an approximately Gaussian shape, i.e.,

$$\omega_z = \omega_o \cdot e^{-\frac{r^2}{R_v^2}} \tag{1}$$

As

$$\omega_z = \frac{1}{r} \cdot \frac{\partial}{\partial r} (r \cdot U_\varphi) \tag{2}$$

one gets

$$U_\varphi = \frac{1}{r} \cdot \int_0^r \omega_z \cdot r' \cdot dr' = \frac{\omega_o \cdot R_v^2}{2 \cdot r} \cdot \left(1 - e^{-\frac{r^2}{R_v^2}}\right) \tag{3}$$

where $R_v = D_v/2$ is the effective radius of the vortex shown in Fig. 3. This Gaussian vortex satisfies the time-dependent Navier–Stokes equations if $\omega_o \cdot R_v^2 = \text{const}$.

The simplified equation of bubble motion used (Sene et al., 1994; Auton et al., 1988) includes only four vector forces, buoyancy (\mathbf{B}), drag (\mathbf{D}), Inertia (\mathbf{I}) and lift (\mathbf{L}), which determine bubble movement in the flow field (see Fig. 3). It reads

$$C_m \frac{d\mathbf{V}_B}{dt} = -\mathbf{g} - \frac{3}{4} \cdot \frac{C_d}{d} \cdot |\mathbf{W}| \cdot \mathbf{W} + (1 + C_m) \cdot \frac{D_L \mathbf{V}_L}{Dt} - C_1 \cdot [\mathbf{W} \times (\mathbf{V} \times \mathbf{V}_L)] \tag{4}$$

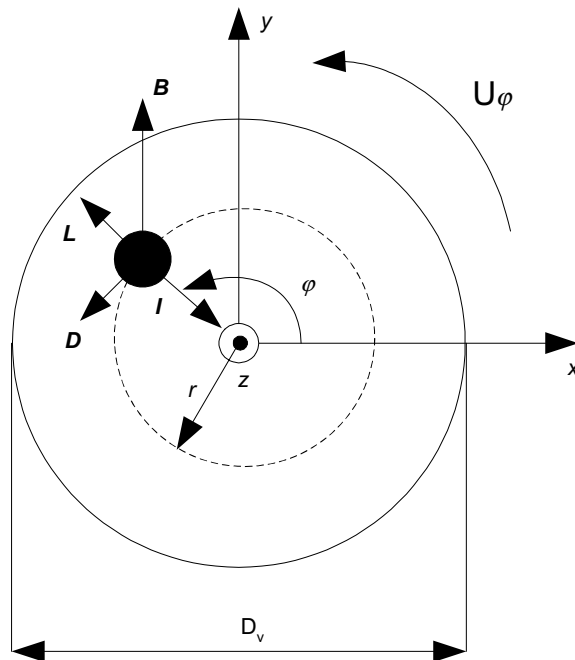


Fig. 3. Forces acting on a single bubble in a vortex.

with

$$\frac{D_L}{Dt} = \frac{\partial}{\partial t} + V_L \cdot \nabla() \quad (5)$$

where the vectors V_L , V_B and $W = V_B - V_L$ are the liquid, bubble and relative velocities, respectively. C_m , C_d and C_l are the added mass, drag and lift coefficients, respectively.

The radial components of L , I , B acting on a bubble at an equilibrium position are

$$L_r = C_l \cdot U_\varphi \cdot \omega_z = C_l \cdot \frac{\omega_o \cdot R_v^2}{2 \cdot r} \cdot \left(1 - e^{-\frac{r^2}{R_v^2}}\right) \cdot \omega_o \cdot e^{-\frac{r^2}{R_v^2}} \quad (6)$$

$$I_r = -(1 + C_m) \cdot \frac{U_\varphi^2}{r} = -(1 + C_m) \cdot \frac{\omega_o^2 \cdot R_v^4}{4 \cdot r^3} \cdot \left(1 - e^{-\frac{r^2}{R_v^2}}\right)^2 \quad (7)$$

$$B_r = g \cdot \cos\left(\varphi - \frac{\pi}{2}\right) = g \cdot \sin \varphi \quad (8)$$

Neglecting the time dependence of the vortex shape, the following condition must be fulfilled at an equilibrium position of the bubble inside the vortex

$$L_r + I_r + B_r = 0 \quad (9)$$

which results in

$$\sin \varphi = (1 + C_m) \cdot \frac{\omega_o^2 \cdot R_v^4}{4 \cdot r^3 \cdot g} \cdot \left(1 - e^{-\frac{r^2}{R_v^2}}\right)^2 - C_l \cdot \frac{\omega_o^2 \cdot R_v^2}{2 \cdot r \cdot g} \cdot \left(1 - e^{-\frac{r^2}{R_v^2}}\right)^2 \cdot e^{-\frac{r^2}{R_v^2}} \quad (10)$$

Similarly, the azimuthal components of B and D are

$$B_\varphi = g \cdot \cos \varphi \quad (11)$$

$$D_\varphi = \frac{3}{4} \cdot \frac{C_d}{d} \cdot U_\varphi^2 = \frac{3}{4} \cdot \frac{C_d}{d} \cdot \frac{\omega_o^2 \cdot R_v^4}{4 \cdot r^2} \cdot \left(1 - e^{-\frac{r^2}{R_v^2}}\right)^2 \quad (12)$$

For equilibrium conditions, the drag coefficient C_d , which, in general, depends on the relative velocity between bubble and liquid, may be replaced by the drag coefficient C_{dT} that corresponds to the terminal velocity of the bubble V_T . Thus with

$$\frac{3}{4} \cdot \frac{C_d}{d} = \frac{g}{V_T^2} \quad (13)$$

where d is the bubble diameter, one obtains

$$D_\varphi = \frac{g}{V_T^2} \cdot \frac{\omega_o^2 \cdot R_v^4}{4 \cdot r^2} \cdot \left(1 - e^{-\frac{r^2}{R_v^2}}\right)^2 \quad (14)$$

For equilibrium

$$B_\varphi + D_\varphi = 0 \quad (15)$$

and therefore

$$\cos \varphi = -\frac{\omega_o^2 \cdot R_v^4}{4 \cdot V_T^2 \cdot r^2} \cdot \left(1 - e^{-\frac{r^2}{R_v^2}}\right)^2 \quad (16)$$

Rearrangement of Eqs. (10) and (16) gives

$$\sin \varphi = \frac{\omega_o^2 \cdot R_v}{4 \cdot g} \cdot f_1\left(\frac{r}{R_v}\right) \quad (17)$$

$$-\cos \varphi = \frac{\omega_o^2 \cdot R_v^2}{V_T^2} \cdot f_2\left(\frac{r}{R_v}\right) \quad (18)$$

with

$$f_1\left(\frac{r}{R_v}\right) = \frac{R_v}{r} \cdot \left(1 - e^{-\frac{r^2}{R_v^2}}\right) \cdot \left[(1 + C_m) \cdot \frac{R_v^2}{r^2} \cdot \left(1 - e^{-\frac{r^2}{R_v^2}}\right) - 2 \cdot C_1 \cdot e^{-\frac{r^2}{R_v^2}} \right] \tag{19}$$

$$f_2\left(\frac{r}{R_v}\right) = \frac{R_v^2}{4 \cdot r^2} \cdot \left(1 - e^{-\frac{r^2}{R_v^2}}\right)^2 \tag{20}$$

In order to be stable, the equilibrium points must lie at $\frac{r}{R_v} < \frac{r_1}{R_v}$ where the function $f_1\left(\frac{r}{R_v}\right)$ has its maximum. This can be shown by checking the direction of the net force acting on a bubble slightly displaced from the equilibrium position. The general trapping criterion can be obtained by noting that

$$\sin^2 \varphi + \cos^2 \varphi = 1 \tag{21}$$

i.e.,

$$Fr_\omega^2 \cdot f_1^2\left(\frac{r}{R_v}\right) + \Gamma_\omega^4 \cdot f_2^2\left(\frac{r}{R_v}\right) = 1 \tag{22}$$

Here, the Vortex Froude number $Fr_\omega = \frac{\omega_o^2 \cdot R_v}{4 \cdot g}$ and the vortex trapping parameter $\Gamma_\omega = \frac{\omega_o \cdot R_v}{V_T}$ have been introduced. They are related by

$$Fr_\omega = \frac{\omega_o^2 \cdot R_v^2}{4 \cdot R_v \cdot g} = \Gamma_\omega^2 \cdot Fr_b \cdot \beta \tag{23}$$

where $Fr_b = \frac{V_T^2}{2 \cdot g \cdot d}$ is the Bubble Froude number and $\beta = \frac{d}{2 \cdot R_v}$ the length scale ratio. Fr_b can be replaced by $\frac{3}{2 \cdot C_{IT}}$. From Eqs. (10)–(23):

$$\Gamma_\omega = \left(\frac{1}{Fr_b^2 \cdot \beta^2 \cdot f_1^2\left(\frac{r}{R_v}\right) + f_2^2\left(\frac{r}{R_v}\right)} \right)^{1/4} \tag{24}$$

$$Fr_\omega = \frac{Fr_b \cdot \beta}{\left(Fr_b^2 \cdot \beta^2 \cdot f_1^2\left(\frac{r}{R_v}\right) + f_2^2\left(\frac{r}{R_v}\right) \right)^{1/2}} \tag{25}$$

Eqs. (24) and (25) relate Γ_ω and Fr_ω to the equilibrium radius r .

The minimum values of Γ_ω and Fr_ω required for trapping are obtained if the maximum allowable value for $\frac{r}{R_v}$ is used. For the usual values of $C_1 = C_m = 0.5$, the functions f_1 and f_2 have their maxima at $\frac{r}{R_v} = 1.027$ and

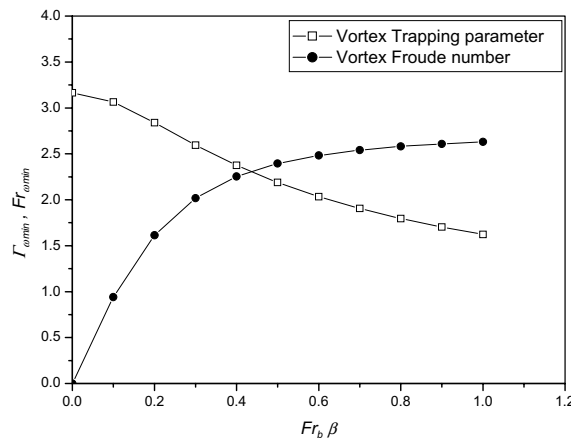


Fig. 4. Minimum values of the vortex trapping parameter and of the Vortex Froude number required for bubble trapping as functions of $Fr_b \cdot \beta$ for $C_1 = C_m = 0.5$.

$\frac{r_2}{R_v} = 1.121$, respectively. For simplicity, $f_1\left(\frac{r}{R_v} = 1\right)$ and $f_2\left(\frac{r}{R_v} = 1\right)$ are used now for calculating the minima of Γ_{ω} and Fr_{ω} that are required for trapping. The results are plotted in Fig. 4 as functions of $Fr_b \cdot \beta$. These results are used for quantifying the bubble trapping condition inside large vortices at different locations in the flow field.

The trapping condition $\Gamma = \frac{\Delta V}{V_T} > 2$ given by Sene et al. (1994), where ΔV is the velocity difference between two fluid streams forming a shear layer, is a simplified form of the more exact bubble-trapping requirement derived here, which depends on bubble and vortex size. The condition can be expressed in terms of either number, Γ_{ω} or Fr_{ω} , and the two quantities are equivalent in this case.

In the discussion by Sene et al. (1994) and Magnaudet and Eames (2000), the effect of vortices on bubble motion are governed by a trapping parameter and by a Froude number which are defined somewhat differently. More explanations can be found in Section 5.1.

With the definition of Γ_{ω} Eq. (24), the minimum value of $\omega_{o,\min}$ required for trapping a bubble inside a Gaussian vortex is

$$\omega_{o,\min} = \Gamma_{\omega,\min} \cdot \frac{V_T}{R_v} \tag{26}$$

Fig. 5 shows $\omega_{o,\min}$ as a function of the bubble diameter and the vortex radius for water at 20 °C and bubbles in the wobbly regime.

Since the vorticity of the liquid phase inside the vortex structures can be directly estimated from PIV measurements, the data presented in Fig. 5 can be used for given bubble and vortex size to estimate quickly whether the conditions for bubble trapping are fulfilled or not.

Magnaudet and Eames (2000) noted that C_d and C_l depend on shear and bubble deformation, so that the trapping condition (Eqs. (24) and (25)) could be affected. In order to discuss the effect of changing C_l , the approximate range within which C_l may vary has to be estimated. According to Magnaudet and Eames (2000), C_l lies between about 0.2 and 0.35 inside a vortex. Experimental data obtained in simple sheared air–water systems (Tomiyama et al., 2002) show that the lift coefficient of small bubbles ($0 < d < 5$ mm) takes values ranging from 0 to 0.3, whereas for big bubbles ($d > 6$ mm) the lift coefficient ranges between 0.15 and -0.3 . In order to illustrate the effect of different values of C_l on the trapping parameter and the Vortex Froude number, a range of $-0.25 < C_l < 0.5$ is chosen and the results plotted in Fig. 6. To obtain the results presented in Fig. 6, the fact that the radius r_1 where the function f_1 reaches its maximum decreases with diminishing C_l has been taken into account. The diagram shows that for negative ($C_l = -0.25$) or vanishing ($C_l = 0$) lift force, bubbles can be more easily trapped than in the case of $C_l = +0.5$.

The effect of shear on C_d can be determined based on results by Legendre and Magnaudet (1998), where it is stated that the drag coefficient increases with shear, i.e.,

$$C_d(Re_b, S) = C_d(Re_b, 0) \cdot (1 + 0.55 \cdot S^2) \tag{27}$$

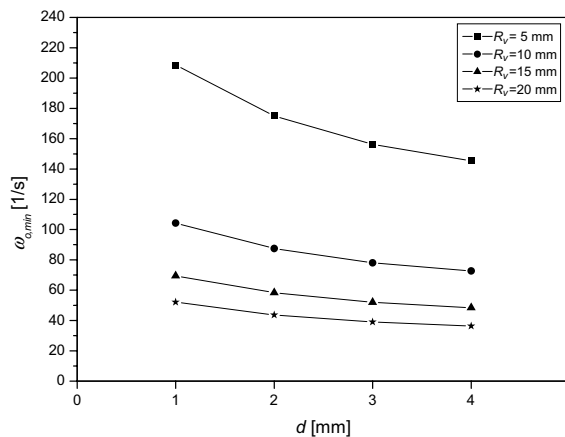


Fig. 5. The minimum value of ω_o required for trapping a single bubble with diameter d inside a Gaussian vortex.

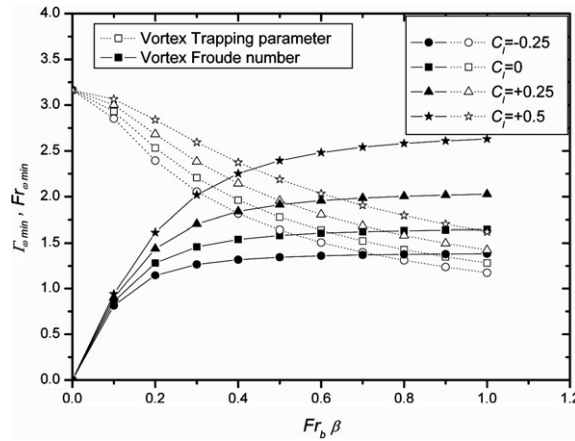


Fig. 6. Effect of the lift coefficient on the vortex trapping parameter and on the Vortex Froude number.

where Re_b is the Bubble Reynolds number

$$Re_b = \frac{|W| \cdot d}{\nu} \tag{28}$$

W is the relative velocity and S , the non-dimensional shear rate, in case of plane shear, is

$$S = \frac{\partial V_L}{\partial x} \cdot \frac{d}{|W|} \tag{29}$$

where V_L is the vertical velocity of the liquid. At an equilibrium position inside a Gaussian vortex, and for cylindrical geometry (Spurk, 1987)

$$S = r \cdot \frac{\partial}{\partial r} \left(\frac{U_\phi}{r} \right) \cdot \frac{d}{U_\phi} \tag{30}$$

and using Eq. (3)

$$S = \frac{d}{2 \cdot R_v} \cdot \frac{4 \cdot R_v}{r} \cdot \left[\frac{r^2}{R_v^2} \cdot \frac{e^{-\frac{r^2}{R_v^2}}}{\left(1 - e^{-\frac{r^2}{R_v^2}}\right)} - 1 \right] \tag{31}$$

The absolute value of S increases almost linearly with $\frac{r}{R_v}$ and reaches the value of $1.672 \cdot \beta$ at $\frac{r}{R_v} = 1$. Thus, the maximum value of the correction factor for C_d is

$$1 + 1.54 \cdot \beta^2$$

For a bubble with $d = 2$ mm inside a vortex with $R_v = 10$ mm (i.e., $\beta = 0.1$) one obtains

$$(1 + 0.55 \cdot S^2) < 1.0154$$

and for a bubble with $d = 6$ mm (i.e., $\beta = 0.3$)

$$(1 + 0.55 \cdot S^2) < 1.138$$

We conclude that the correction factor for C_d does not significantly change the trapping condition, but it facilitates trapping in all cases.

The discussion of flow-induced changes of C_l and C_d shows that bubble deformation and shear tend to promote trapping, although the vortex region where equilibrium of forces can exist decreases if C_l is reduced.

5. Experimental results for naturally developing jets

Experimental results for naturally developing jets are presented to make the advantages of triggering the jet evident and to compare data for naturally-developing and triggered jets. These results also show what happens if the trapping conditions are not fulfilled and therefore represent a baseline for further study of triggered jets. The data were obtained for a turbulent bubbly jet with mean superficial liquid velocity at the nozzle exit, $V_{\text{jet}} = 0.45$ m/s, homogeneous void fraction of 3.4% and bubble diameter d of about 2 mm. This test condition was initially chosen to create an inertia-dominated flow with the highest possible values of the non-dimensional parameters that could be achieved with the existing water pump and the installed jet nozzle ($D = 90$ mm).

The trapping conditions defined by Sene et al. (1994) were not fulfilled at a downstream distance from the nozzle of $4D$ where the large vortices reach their maximum strength (Crow and Champagne, 1971) because the Froude number $Fr_v = \frac{V_{\text{jet}}^2}{2g\delta}$ (where δ is the characteristic vortex diameter, which equals $D/2$ at a distance $4D$ from the nozzle exit (Crow and Champagne, 1971)), was less than 1 and the trapping parameter $\Gamma = \frac{V_{\text{jet}}}{V_T}$ (where V_T is the terminal bubble rise velocity), was only about 1.7. Despite this, the flow regime was investigated to examine whether bubble trapping could be found closer to the nozzle exit where the vortex diameter δ is smaller and the local Fr_ω and Γ_ω would possibly be large enough.

Profiles of the mean vertical velocity of the bubbles and of the liquid obtained by PIV are presented in Fig. 7a. Bubbles have higher velocity than the liquid at all downstream positions in the shear layer, which appears to indicate that they are not trapped inside large structures formed in the mixing layer. One has to add, however, that only a fraction of the bubbles that would be detected at radial positions of the jet where large vortices occur can be trapped inside such vortices.

The azimuthal vorticity presented in Fig. 7b is produced by the mean shear. Its maximum in the shear layer at $y = 100$ mm ($y/D = 1.12$) from the nozzle exit is about 25 s^{-1} . The thickness of the shear layer is about 25 mm. If one assumes that the radius of the large structures in the shear layer corresponds to half its thickness, the non-dimensional parameters presented above can be calculated in order to check the trapping conditions. The terminal rise velocity for 2 mm bubbles is about 0.3 m/s. Based on these values, the vortex trapping parameter is 1.03, while the Vortex Froude number is 0.18. The minimum values required for trapping bubbles inside a Gaussian vortex with a radius of 12.5 mm calculated with the criteria presented above, are 2.9 for the vortex trapping parameter and 1.5 for the Vortex Froude number. Basically the trapping conditions are not fulfilled. However, as the random formation of larger vortices is possible, the peak vorticity inside these structures can be expected to be higher than the mean value.

The results thus prove that significant and evident bubble trapping could not be found in the chosen case. In order to fulfil the trapping condition, jet flow conditions with higher values of Froude number and trapping parameter must be reached.

5.1. Statistical analysis of DOS results

In order to test whether bubble clustering could be detected by the DOS, a statistical analysis was conducted to show whether the number of bubbles hitting the probe per time interval deviates from that of a probabilistically uniform bubble density distribution. A second goal was to find whether the bubble velocity depended on the bubble density or the corresponding void fraction obtained by averaging over small time intervals.

Since the void fraction is given by the time fraction during which bubbles contact the sensor, it is obvious that, if the measurement-time intervals are small, this “void fraction” fluctuates stochastically between 0 and 1 and no longer has the original physical meaning of volumetric void fraction. However, the number of bubbles hitting the sensor per time interval can be precisely counted and statistically analyzed. Correlations of detected “void fractions” with appertaining bubble velocities are presented for a location in the shear layer at $x = +50$ mm and $y = 350$ mm ($y/D = 3.9$), Fig. 8.

The statistical analyses of the experimental data have been performed by dividing the total measuring period into intervals of 0.02 s or 0.1 s. If the mean bubble velocity is about 0.6 m/s, the DOS data, that are averaged over a time interval of 0.02 s are thus effectively averaged over a vertical distance of 12 mm whereas the

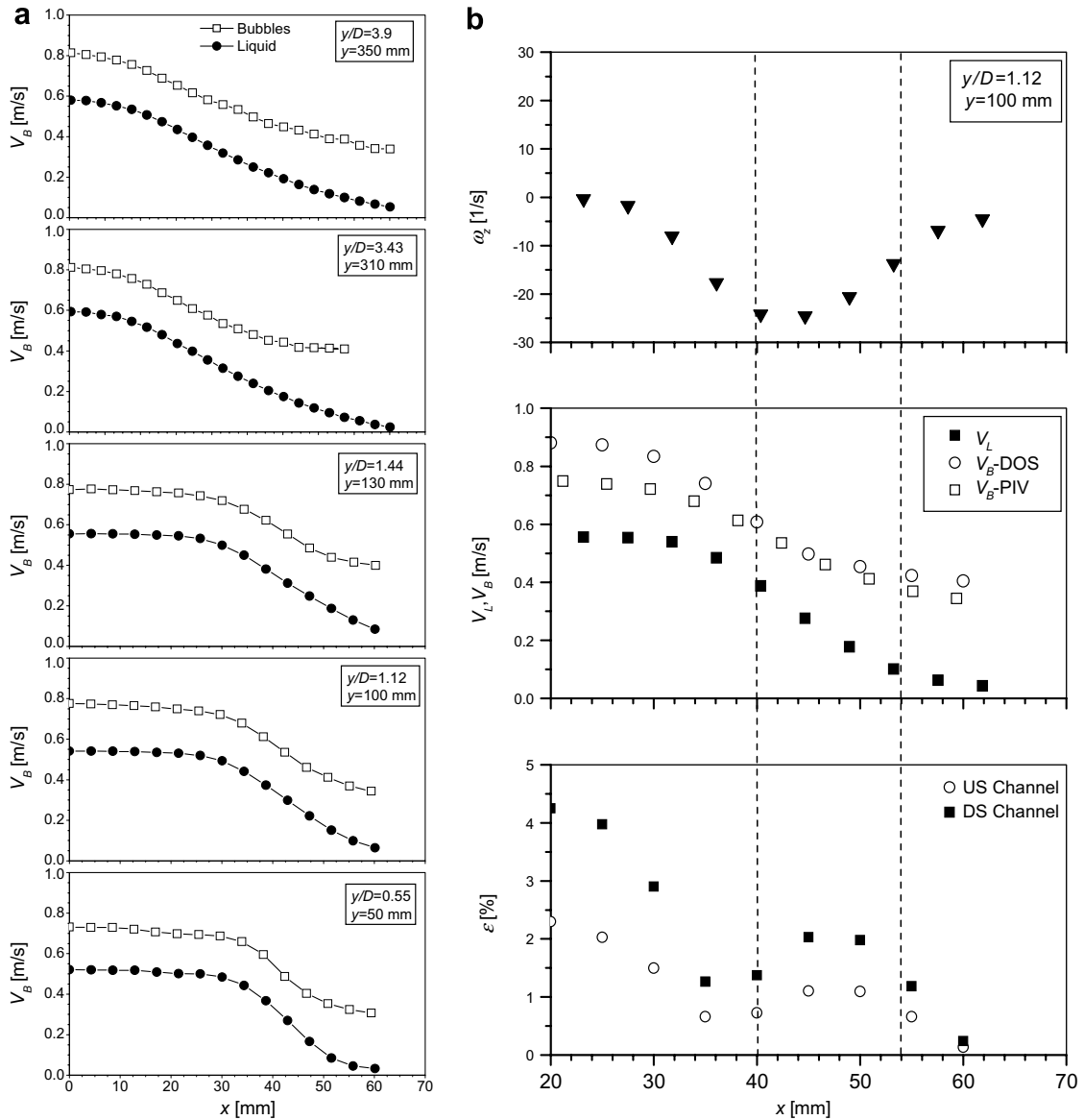


Fig. 7. (a) Downstream development of the horizontal profiles of the vertical bubble and liquid velocities obtained by PIV. (b) Vertical-velocity profiles of the bubbles, obtained by DOS and PIV, and of the liquid, obtained by PIV (middle); void fraction profiles obtained by downstream optical probe tip (DS) and upstream optical probe tip (US) (bottom); and azimuthal vorticity profile (top) at $y = 100$ mm from the nozzle exit.

time interval of 0.1 s corresponds to a vertical distance of 60 mm. Thus, assuming that the diameter of the large vortices is about 25 mm, the time interval of 0.1 s is too large for resolving bubble structures produced by these vortices, but as mentioned before, a smaller time interval means that there are fewer events available for averaging and therefore, void fractions obtained by integrating the bubble signals over small time intervals vary within a very wide range.

Since the total number of bubbles in the shear layer is considerably smaller than at the jet centre, the longer time intervals were chosen there to increase the probability of detecting more than one bubble per time interval.

The correlation between bubble velocity and void fraction is presented in Fig. 8a for a point in the shear layer. Although the “void fraction” and bubble velocity data are correlated in this case, this result is not

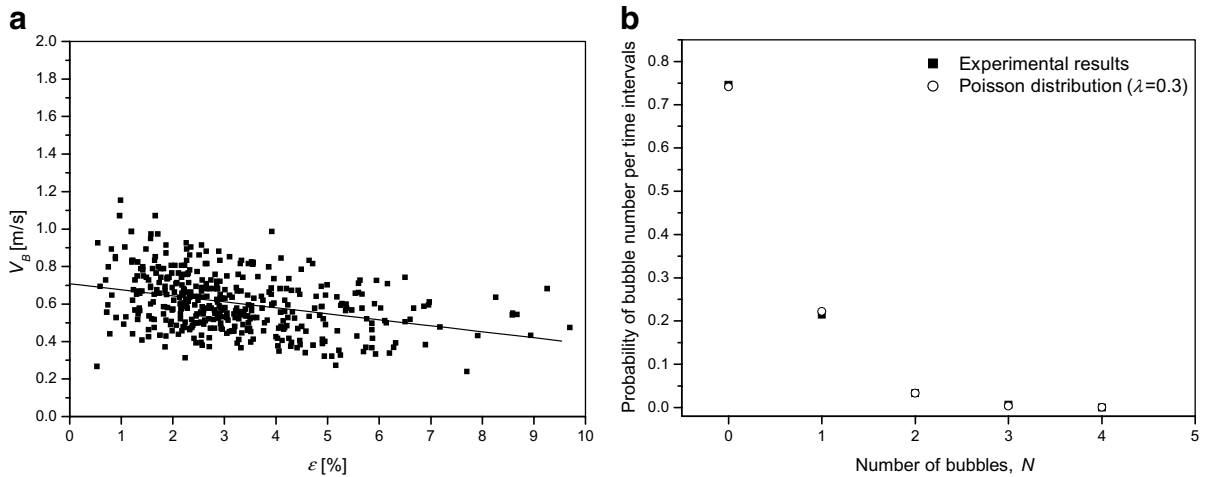


Fig. 8. (a) Correlation between velocity and void fraction at $x = +50$ mm, $y = 350$ mm (interval of 0.1 s) and (b) probability of detecting N bubbles per time interval of 0.1 s for the point at $x = +50$ mm and $y = 350$ mm.

produced by the mean shear because the measured velocity decreases with ε , opposite to the effect that the mean shear would have, because fluid lumps coming from inside the jet contain more bubbles and have higher axial velocity than those coming from outside. The real reason for the observed correlation lies in the fact that the bubble residence times are not short compared to the integration time interval of 0.1 s. Slow bubbles with long residence times give rise to large ε values since the probability that more than one bubble is detected in a time interval is relatively small, independent of the velocity.

The probability of detecting N bubbles per time interval and a comparison with a Poisson distribution are presented in Fig. 8b. The figure does not show a significant deviation from the Poisson distribution, although this may be caused by the too-small probability of detecting more than one bubble per time interval. In order to find a deviation from the Poisson distribution, a larger bubble density would have been required for the given time interval. These statistical analyses of DOS measurements thus do not show any clustering of bubbles in the shear layer of naturally-developing jets and the apparent correlation between ε and V_B is only a fortuitous result.

It is obviously very difficult to obtain information on the size and the development of the large eddy structures in naturally-developing flows, as well as to quantify the interaction between bubbles and the large vortices that are formed in the shear layer. For correlating flow characteristics such as bubble and liquid velocities, as well as void fraction, it would have been necessary to develop new or to improve existing experimental techniques for the simultaneous measurement of these quantities. The simultaneous PIV measurements that were performed during this study represent a very first, basic step as they resolve only the velocity fields in two-phase flow. Processing of the images to also obtain information on bubble concentration inside the interrogation area could, however, be a tempting task for future investigations.

If, however, coherent structures are periodically produced, bubble movements inside these structures can be systematically analysed. In order to investigate the possibility of using the DOS technique to obtain phase-averaged void fraction and bubble velocity data, the triggered experiment presented in the next section was conducted.

6. Experimental results for triggered jets

The results presented now ($St = 0.6$, $f = 2$ Hz (Milenkovic, 2005)) were obtained for a turbulent bubbly jet with mean superficial liquid velocity at the nozzle exit of $V_{jet} = 0.32$ m/s, homogeneous void fraction of 3.4% and bubble diameter of about 4 mm. The analytical approach (Section 4.1) shows that large bubbles can be more easily trapped inside Gaussian vortices than small ones because they require smaller vorticity. This is mainly due to the reduced strength of the lift force (see discussion on the variation of the lift coefficient C_L

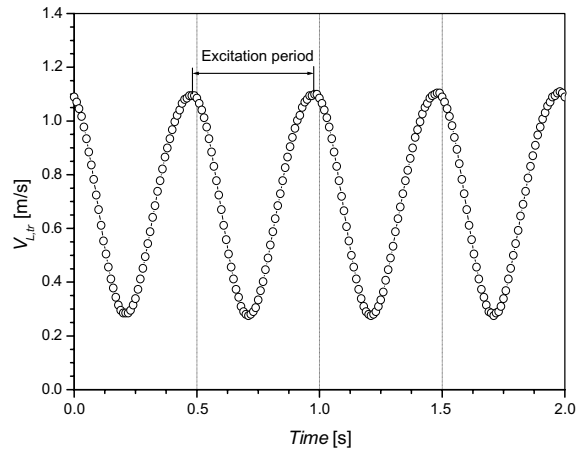


Fig. 9. Modulated excitation velocity at the exit of the triggering nozzle for case f_2 (2 Hz).

with bubble diameter in Section 4.1). Therefore, bubbles with diameter of 4 mm instead of 2 mm, as in the experiment with a naturally-developing jet, were used now. The triggering frequency f , which corresponds to a Jet Strouhal number $St = \frac{Df}{V_{\text{jet}}} = 0.6$, was 2 Hz. Earlier tests performed with triggered single-phase jets (Milenkovic, 2005) indicated that forcing at higher Strouhal number raises the peak vorticity and reduces the distance between two consecutive vortex rings. The Jet Reynolds number was $Re_{\text{jet}} = \frac{V_{\text{jet}} D}{\nu} = 30275$.

The variation of the triggering-velocity for this test is presented in Fig. 9. It is the velocity of the excitation flow at the exit of the triggering nozzle, obtained from the measured modulated flow rate.

6.1. Bubble ring

Bubble trapping is the condition of bubbles reaching an equilibrium position within the vortices (as defined in Section 4.1) and travelling with them at the same velocity. If a sufficient number of bubbles reach such positions in the toroidal vortices, a bubble ring is formed. The photograph of Fig. 10 illustrates this phenomenon. The generation of a bubble ring (Fig. 11) that travels with the same velocity as the vortex is a clear indication of bubble trapping inside the vortex. The velocities of both vortex and bubble ring can be estimated from the data acquired by the PIV vortex tracking method with or without illumination of the flow field with back-light (for more details see Milenkovic et al., 2005; Milenkovic, 2005). Visualization tests were conducted by injecting fluorescent dye in the vortices (white clouds in Fig. 11). These pictures show strong deformations of the bubble ring (Fig. 11).



Fig. 10. Perfectly aligned bubbles in a bubble ring.

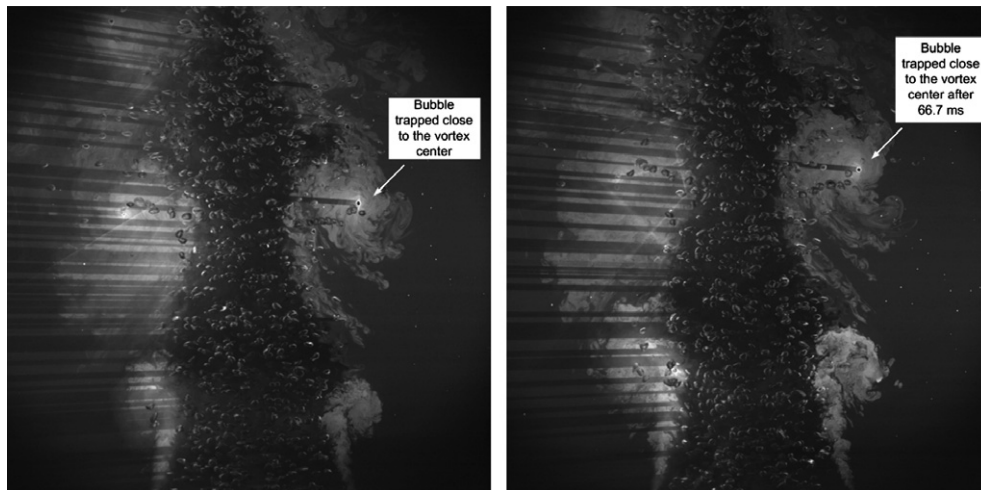


Fig. 11. Sequence of two photos of the vortex ring with bubble trapped close to the vortex center. The pictures, acquired with time interval of 66.7 ms, show almost the same position of the trapped bubble close to the vortex center, which means that it travels downstream at the same vertical velocity as the vortex.

6.2. Phase-averaged velocity fields obtained by PIV

A typical result for the vorticity field obtained by PIV when the centre of the vortex ring lies at $y \approx 100$ – 105 mm is shown in Fig. 12. The position of the bubble ring for this phase is shown in Fig. 11. Phase-averaged profiles of the vertical velocity of the bubbles (V_B) and of the liquid (V_L), as well as of the azimuthal vorticity below and across the vortex ring (at $y = 84, 91, 98$ and 105 mm), are presented in Fig. 13. The vortex centre on the right side is at about $y = 105$ mm. These data are presented in order to compare bubble and liquid velocities in and below the vortex ring and to check whether the simplified criterion for bubble trapping (Section 4.1) is fulfilled or not.

The velocity of the bubbles inside the vortex ring at $x \approx 60$ mm is in this case higher than the liquid velocity at the same x -coordinate and about the same as the vertical velocity of the vortex centre (about 0.26 m/s), obtained by the vortex tracking method mentioned above. This indicates that the bubbles are trapped at this location and they travel with the same velocity as the vortex ring. In order to check whether the analytical

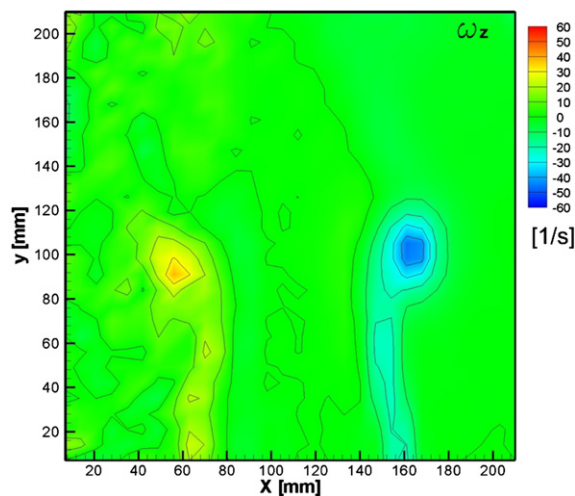


Fig. 12. Phase-averaged azimuthal vorticity of the liquid. The jet centerline is at $X = 108$ mm.

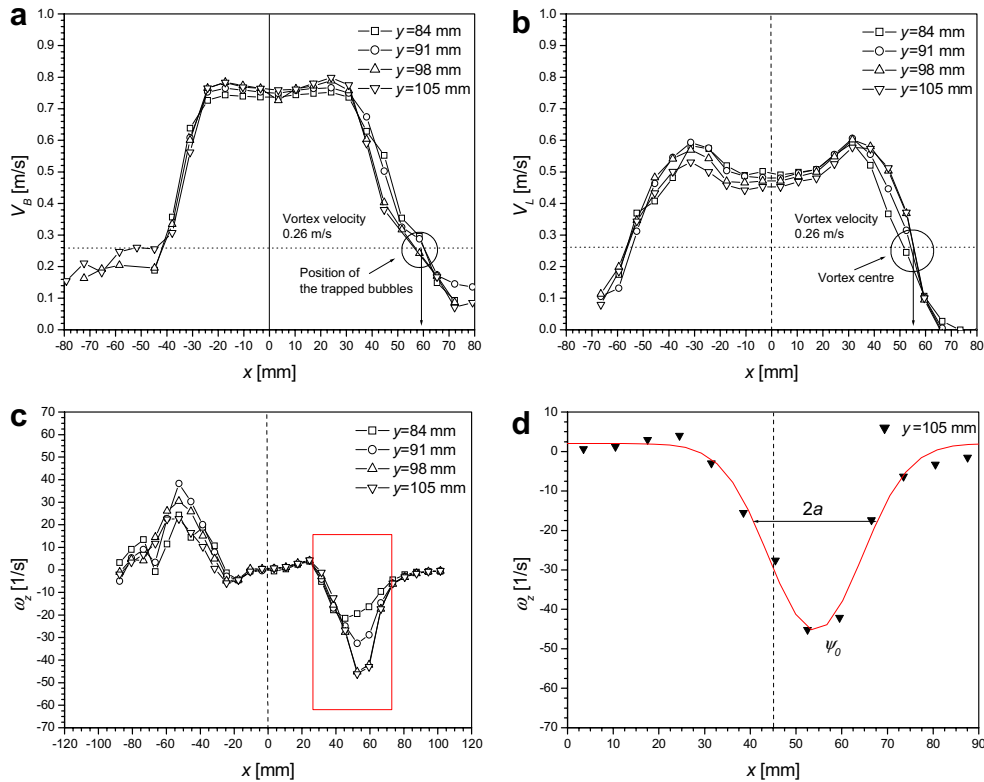


Fig. 13. Phase-averaged velocity profiles of the bubbles (a), of the liquid (b), and of the azimuthal vorticity of the liquid (c). Gaussian fit of the azimuthal vorticity of the liquid across the vortex center (d).

trapping conditions are fulfilled, the size of the vortex and the maximum vorticity at the vortex center have to be estimated. Fig. 13d shows a Gaussian fit of the azimuthal vorticity of the liquid through the vortex centre at $y = 105$ mm. Measured maximum vorticity at the vortex centre is about -48 s^{-1} . The vortex radius estimated from this fit is about 15 mm. The terminal bubble rise velocity for 4 mm bubbles is 0.24 m/s. Based on these values, the vortex trapping parameter is 3 and the Vortex Froude number 0.88. The minimum values required for trapping of bubbles inside a Gaussian vortex with radius of 15 mm based on the criteria presented above (Fig. 4) are 3.1 for the vortex trapping parameter and 0.92 for the Vortex Froude number. Thus, the trapping conditions are fulfilled.

6.3. Phase-averaged void fraction and vertical bubble velocity measured by DOS

DOS data have been acquired for the same flow conditions at the elevations $y = 100$ mm and $y = 200$ mm for points in the jet centre, at the jet boundaries, and in the shear layer (Milenkovic, 2005). Only the results from the shear layer are discussed here.

As already mentioned above, in order to obtain a statistically sufficient number of events, especially for points located in the low-bubble concentration regions (in the shear layer), the total number of excitation periods used for phase-averaging must be high. This means very long measurement times, fairly high demands on DOS signal stability and high-precision hardware. Therefore, data acquisition was carried out for 6000 excitation periods for points with low-bubble concentration and for 3000 periods for points with higher bubble concentration. Each excitation period of 0.5 s was subdivided into 25 intervals of 0.02 s. The bubble number, void fraction and bubble vertical-velocity data were phase-averaged for each of the intervals.

Experimental results at two different locations, $y = 100$ mm and $y = 200$ mm at the boundary of the shear layer ($x = 45$ mm) are presented in Fig. 14. At this radius, shear-layer vortices entrain bubbles together with

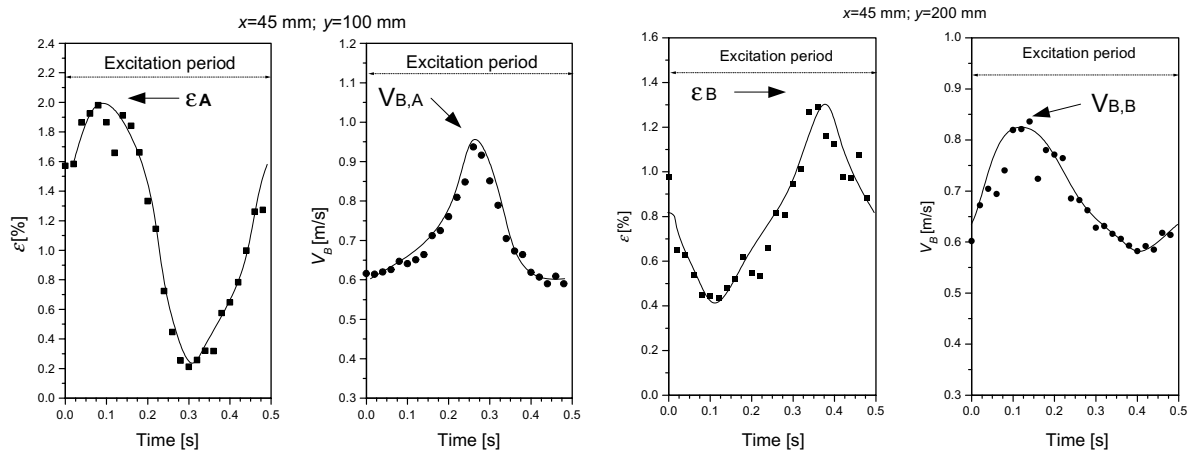


Fig. 14. Variations of the void fraction and of the vertical bubble velocity during the excitation period at two different elevations in the shear layer, at $y = 100$ mm and 200 mm.

the liquid into the mixing region. The results show the time-dependence of the phase-averaged bubble velocity and of the void fraction during an excitation period. The phase-averaged DOS data indicate bubble clustering correlated with coherent vortex structures. The bubble velocity points ($V_{B,A}$ and $V_{B,B}$) peaks at times when a minimum void fraction is measured. The interrelation between vertical bubble velocity and void fraction shows the influence of the liquid velocity field outside the vortex rings. The increased bubble concentration during certain phases is mainly caused by a bubble wave driven radially outward ahead of the large vortices, while low concentration indicates phases where the sensor tips are inside the zone behind the bubble wave. The bubbles that arrive at the sensor tip have different mean velocity and direction of flow at different phases of the excitation period. The apparently high-bubble velocity prevailing during the low-void phase (Fig. 14) could be caused by the shear layer pulsation. The bubble velocity measurements conducted by DOS may, however, have been partly impaired by the biasing effect resulting from the non-alignment of probe tips and bubble velocity direction, as discussed by Milenkovic (2005).

The time delay between the void fraction maxima (ε_A and ε_B) at the two different elevations in Fig. 14, measured at the same radial position in the shear layer ($x = 45$ mm), is about 0.28 s for the vertical distance of 100 mm. The resulting downstream travelling velocity of the bubble wave of 0.36 m/s is distinctly higher than the value for the vortex velocity obtained by PIV. This difference indicates that the bubble density wave appears to drift relative to the coherent liquid vortices.

Experimental results for points in the shear layer at $x = 45, 53, 54, 57, 62$ and 66 mm and $y = 100$ mm are presented in Fig. 15. The results show that the void fraction decreases towards the boundaries of the jet, as expected. The void fraction peaks, especially for the points at $x = 62$ mm and 66 mm, may correspond to trapped bubbles, i.e., bubbles which belong to the bubble ring. The PIV data presented in Fig. 12 show that these points are located close to the vortex centre where bubble trapping occurs.

DOS results for the points at $x = 45, 53, 54$ and 57 mm indicate a strong variation of the bubble density. These points are located in a region of the vortex where bubbles are not expected to be trapped. Based on PIV data, the latter three points are very close to the vortex centre, where few bubbles can be trapped. The shapes of the periodic void fraction variation at different axial locations in the shear layer are just shifted in time and differ in amplitude. Obviously, PIV and photographic recordings would be needed to fully record the bubble and liquid velocity fields and to show how they interact. The results provide quantitative information on the development of a periodically triggered bubbly jet and can be used for comparisons with results of time-dependent LES (Large Eddy Simulation) calculations for the same flow and boundary conditions.

Experimental results for points in the shear layer at $x = 45, 47, 49, 51, 53$ and 55 mm at the higher elevation, $y = 200$ mm are presented in Fig. 16. A strong variation of the bubble density is still visible for all x -coordinates, but the mixing process in the shear layer causes the void fraction to become temporally more uniform than at $y = 100$ mm, especially for $x > 50$ mm.

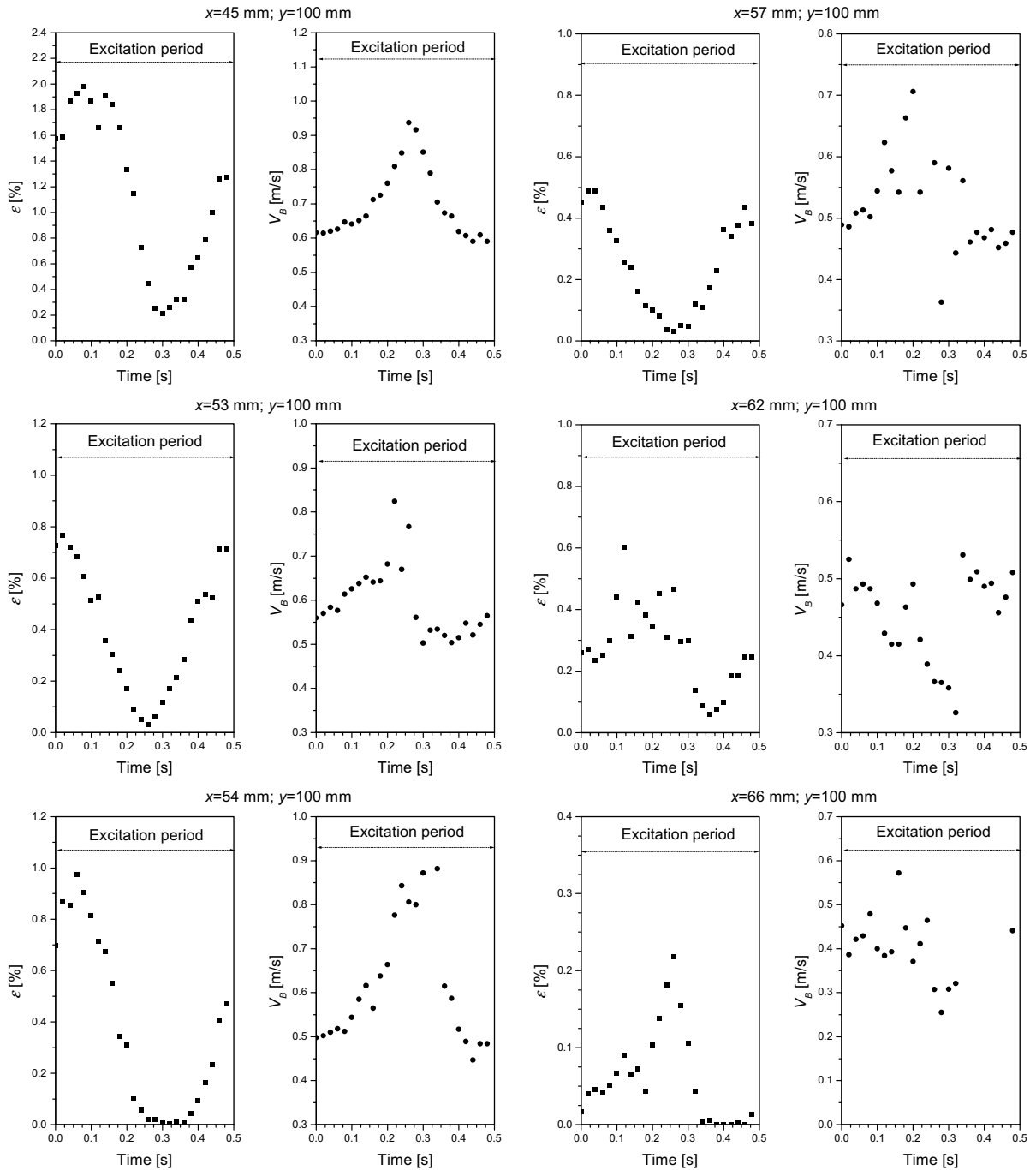


Fig. 15. Variation of the void fraction and of the vertical bubble velocity during the excitation period (for points in the shear layer at $y = 100$ mm).

The periodic variation of the void fraction clearly indicates the existence of coherent bubble structures in the shear layer, but bubble trapping cannot be detected by the DOS technique alone. It can only be shown that the measurements are consistent with the PIV results if bubble trapping occurs.

The greatest profit of the phase-averaged DOS measurements are the results for space- and time-dependent, coherent bubble densities or void fractions that are produced with adequate spatial resolution. Indeed the

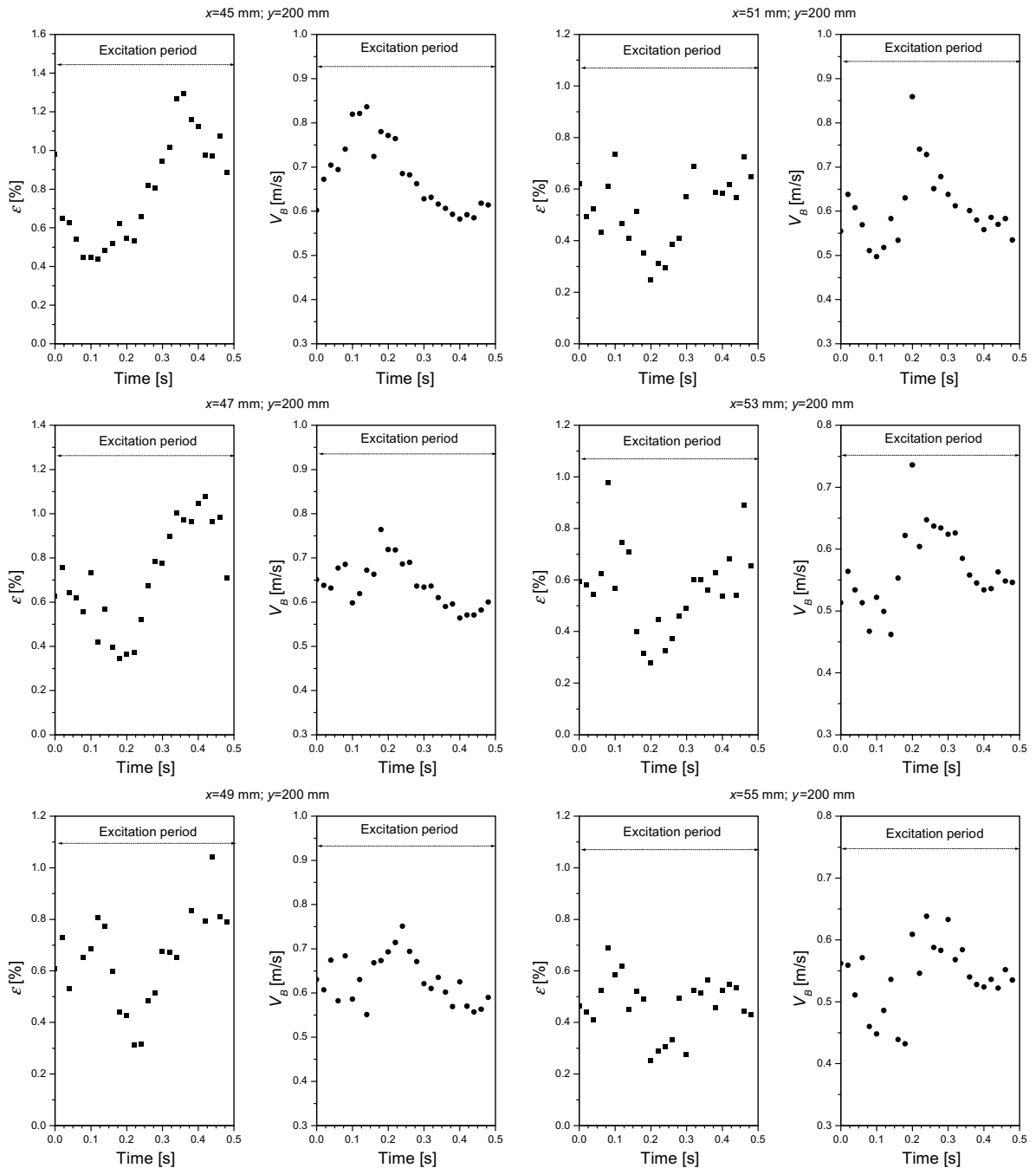


Fig. 16. Variation of the void fraction and of the vertical bubble velocity during the excitation period (for points in the shear layer at $y = 200$ mm).

temporal resolution achieved with the optical sensors is higher than the temporal resolution of the PIV system, which is restricted to 15 Hz. For instance, the production of PIV data with, e.g., 25 time steps per excitation period of 0.5 s cannot be obtained in a single PIV run with a maximum available frequency of 15 Hz. This could only be produced in a series of tests with different phase shifts between vortex excitation and PIV shots. It is obvious that the performance and analysis of such series of runs would be very time-consuming and it would have been difficult to ensure reproducibility of all relevant experimental conditions along the runs.

The value of this kind of results is also limited in that only the coherent part of the fluctuations can be correlated. The development of a photographic technique that enables void (or bubble density) measurements simultaneously with the PIV experiments is a suggestion for future work.

7. Conclusions

The dispersion of bubbles in shear layers is effected by the momentum transfer between bubbles and liquid in two-phase flow resulting from the different forces acting on the bubbles. Experiments carried out with variable inlet conditions provide quantitative information on the development of a periodically-triggered bubbly jet and can be used to examine the adequacy of the various models for momentum transfer between bubbles and the liquid field that are used in time-dependent LES calculations.

Controlled excitation at fixed frequency and with defined amplitude, achieved by producing small flow surges around the jet nozzle, causes large eddy structures to develop at regular intervals. The synchronization with data acquisition is found to be a useful tool for the observation of bubble movement that cannot be achieved in naturally-developing jet flows.

The PIV technique, combined with a photographic technique using backlighting, enables identification of bubble trapping and verification of the required trapping conditions which can be expressed in terms of either the vortex trapping parameter, Γ_ω or the Vortex Froude number Fr_ω .

The phase-averaged void fraction, bubble velocities and bubble numbers obtained by DOS show the existence of coherent structures in the shear layer. In order to quantify bubble trapping, however, DOS phase-averaged data must be combined with phase-averaged PIV data.

Acknowledgements

The authors gratefully acknowledge the support of the project by the Swiss National Science Foundation under contract No. 200020-103630 and wish to thank Max Fehlmann for his helpful assistance and numerous technical contributions to the design and erection of the experimental installation.

References

- Auton, T.R., Hunt, J.C.R., Prud'Homme, M., 1988. The force exerted on a body in inviscid unsteady non-uniform rotational flow. *J. Fluid Mech.* 197, 241–257.
- Crow, S.C., Champagne, F.H., 1971. Orderly structure in jet turbulence. *J. Fluid Mech.* 48, 547–591.
- Dantec Dynamics, 2000. Flow Manager Software and Introduction to PIV Instrumentation.
- Druzhinin, O.A., Elghobashi, S.E., 2001. Direct numerical simulation of a three-dimensional spatially developing bubble-laden mixing layer with two-way coupling. *J. Fluid Mech.* 429, 23–61.
- Huerre, P., Monkewitz, P.A., 1985. Absolute and convective instabilities in free shear layers. *J. Fluid Mech.* 159, 151–168.
- Hussain, A.K.M.F., 1983. Coherent structures, reality and myth. *Phys. Fluids* 26, 2816–2850.
- Hussain, A.K.M.F., Zaman, K.B.M.Q., 1981. The preferred mode of the axisymmetric jet. *J. Fluid Mech.* 110, 39–71.
- Hussain, A.K.M.F., Zaman, K.B.M.Q., 1980. Vortex pairing in a circular jet under controlled excitation – Part 2: Coherent structure dynamics. *J. Fluid Mech.* 110, 493–544.
- Kubasch, J., 2001. Bubble Hydrodynamics in Large Pools. Doctoral Thesis No. 14398. ETH Zürich, Switzerland.
- Le Corre, J.M., Ishii, M., 2002. Numerical evaluation and correction method for multi-sensor probe measurement techniques in two-phase bubbly flow. *Nucl. Eng. Des.* 216, 221–238.
- Legendre, D., Magnaudet, J., 1998. The lift force on a spherical bubble in a viscous linear shear flow. *J. Fluid Mech.* 368, 81–126.
- Magnaudet, J., Eames, I., 2000. The motion of high-Reynolds-number bubbles in inhomogeneous flows. *Ann. Rev. Fluid Mech.* 32, 659–708.
- Mastorakos, E., Shibasaki, M., Hishida, K., 1996. Mixing enhancement in axisymmetric turbulent isothermal and buoyant jets. *Exp. Fluids* 20, 279–290.
- Milenkovic, R., 2005. Experimental Investigation of Bubbly Jets. Doctoral Thesis No. 16206. ETH Zürich, Switzerland.
- Milenkovic, R., Fehlmann, M., 2005. Gas/liquid injector (mass and/or heat transfer apparatus and method for mass and/or heat transfer enhancement). Pending EU/USA Patent (PSI and ETHZ patent application No. 2003P19217EP (F-5125)).
- Milenkovic, R., Sigg, B., Yadigaroglu, G., 2005. Study of periodically excited bubbly jets by PIV and double optical sensors. *Int. J. Heat Fluid Flow* 26, 922–930.
- Papanicolaou, P.N., List, E.J., 1988. Investigations of round vertical turbulent buoyant jets. *J. Fluid Mech.* 195, 341–391.
- Raffel, M., Willert, C., Kompenhans, J., 1998. Particle Image Velocimetry – A Practical Guide. Springer.

- Rightley, P.M., Lasheras, J.C., 2000. Bubble dispersion and interphase coupling in a free-shear flow. *J. Fluid Mech.* 412, 21–59.
- Ruetsch, G.R., Meiburg, E., 1993. On the motion of small spherical bubbles in two-dimensional vortical flows. *Phys. Fluids A* 5, 2326.
- Sene, K.J. et al., 1994. The role of coherent structures in bubble transport by turbulent shear flows. *J. Fluid Mech.* 259, 219–240.
- Spurk, J.H., 1987. *Stroemungslehre*. Springer, pp. 420–422.
- Tomiya, A., Tamai, H.C., Zun, I., Hosokawa, S., 2002. Transverse migration of single bubbles in simple shear flows. *Chem. Eng. Sci.* 57, 1849–1858.
- Ullum, U., Schmidt, J.J., Larsen, P.S., McCluskey, D.R., 1998. Statistical analysis and accuracy of PIV data. *J. Visual.* 1, 205–216.
- Zaman, K.B.M.Q., Hussain, A.K.M.F., 1980. Vortex pairing in a circular jet under controlled excitation – Part 1: General jet response. *J. Fluid Mech.* 101, 449–491.